Dynamics of Water Trapped between Hydrophobic Solutes

Niharendu Choudhury[†] and B. Montgomery Pettitt*

Department of Chemistry, University of Houston, Houston, Texas 77204-5003

Received: October 6, 2004

We describe the model dynamical behavior of the solvent between two nanoscopic hydrophobic solutes. The dynamics of the vicinal water in various sized traps is found to be significantly different from bulk behavior. We consider the dynamics at normal temperature and pressure at three intersolute distances corresponding to the three solvent separated minima in the free energy profile between the solutes with attractions. These three states correspond to one, two, and three intervening layers of water molecules. Results are obtained from a molecular dynamics simulation at constant temperature and pressure (NPT) ensemble. Translational diffusion of water molecules trapped between the two solutes has been analyzed from the velocity correlation function as well as from the mean square displacement of the water molecules. The rotational behavior has been analyzed through the reorientational dynamics of the dipole moment vector of the water molecule by calculating both first and second rank dipole−dipole correlation functions. Both the translational and reorientational mobilities of water are found to be much slower at the smaller separation and increases as the separation between solutes becomes larger. The occupation time distribution functions calculated from the trajectories also show that the relaxation is much slower for the smallest intersolute separation as compared to other wider separations. The sublinear trend in mean square displacement and the stretched exponential decay of the relaxation of dipolar correlation and occupation distribution function indicate that the dynamical behavior of water in the confined region between two large hydrophobic solutes departs from usual Brownian behavior. This behavior is reminiscent of the behavior of water in the vicinity of protein surface clefts or trapped between two domains of a protein.

I. Introduction

It is well recognized[1−5] that water plays an important role in determining the structure, function and dynamics of biological macromolecules. Many biological molecules are inactive without a threshold level of hydration.[6−8] Macromolecules associate by merging the solvation layers at each surface, subsequently making contact or often sharing water molecules at the interface.[9] We wish to better understand the differences in the dynamics of water near surfaces at different distances.[10] How water responds dynamically when trapped may give indications about the proposed mechanisms[11] for stability of hydrophobics in solution.

The water molecules in the vicinity of a biomolecule may be divided into three categories, viz., (i) internal water, which are fairly immobilized in the solute molecule, (ii) hydration water, which stays for some time in the hydration shell of a solute molecule, and (ii) bulk water, which is far away from the solute surface. Hydration waters being close to the protein surface, interact with the atoms in the protein surface, but they are not as immobilized as the interior waters. These molecules frequently get exchanged with those from the bulk region and occasionally with those on the interior. However, they are not as free as bulk water as far as their positions and motions are correlated with the biomolecule. Hydration water thus plays a crucial role not only in determining structure and dynamics of a biomolecule but also in determining its chemical and structural activities as well.

The structural and dynamical behavior of hydration water in the immediate vicinity or trapped between two regions of a bio macromolecule are also believed[12−16] to have considerable importance in determining the mechanism of folding of a protein molecule. The interior of a protein is often hydrophobic in nature. Given the complicated surface topography and chemical heterogeneity of a protein surface, it is of interest to consider the structure and dynamics of water near a large model hydrophobic surface to better understand this aspect of macromolecular association and assembly.

There are several recent theoretical[11,17−19] as well as simulation[20−23] studies in the literature concerning the role of hydrophobic effect on the solvent induced collapse and/or aggregation of proteins. Several such studies use model hydrophobic surfaces. In such an investigation on the hydration of two large model ellipsoidal solutes, Berne and co-workers[22] have reported a dewetting induced collapse of the two solutes in water. They found a complete expulsion of water molecules or drying between two solutes at a critical intersolute separation of around 14 Å, when they considered a purely repulsive solute−water interaction. However, a sharp decrease in this critical distance for dewetting is observed when they considered even a very weak attractive interaction for the solute−solvent potential. In a very recent study,[24] we have shown by calculating the free energy of hydration as a function of the surface to surface distance, how the mechanism of the hydration forces between large hydrophobic solutes is different depending on the strength of solute−solvent attraction and the size of the solutes.

Earlier studies left unresolved issues related to surface curvature and potential models. To separate the issues, we

* Corresponding author. Fax: +1-713-743-2709. E-mail: pettitt@uh.edu.
[†] On leave from RC & CD Division, Bhabha Atomic Research Centre, Mumbai 400 085, India. E-mail: niharc2002@yahoo.com.

10.1021/jp045439i CCC: $30.25 © 2005 American Chemical Society
Published on Web 03/15/2005

considered first flat platelike solutes of various dimensions. Using fully atomic descriptions of the solutes modeled as a graphite-like plates made up of carbon atoms, we found a dewetting at an intersolute separation of 10 Å only if a purely repulsive water−solute interaction is considered. However, using a reasonable dispersion parameter taken from a popular force field[25] for the carbon atoms of the solute, it was shown[24] that the cumulative effect of a large number of small attractive interactions of the solute with water can stabilize the solvent separated state containing as little as one layer of water molecules between the two large solutes without any cavitation or drying. Although energy loss due to disruption in the hydrogen bond network in water may not, in general, favor[11] the dissolution process of a large hydrophobic solute, a delicate interplay between solute−solvent and solute−solute attractive interaction and lost hydrogen bond energy determines the stability of such a state.

The mechanisms for the stabilization of the solute contact pair in the cases with and without small dispersion attractions were shown[24] to be strikingly different. For the purely repulsive solute, the contact pair is stabilized completely by a large negative free energy contribution from the solvent induced interaction, whereas for a solute with weak attraction for the solvent, the contact pair is mainly stabilized by the solute−solute interaction, with the solvent induced contribution providing barriers between minima and being negligibly small at contact. This behavior is consistent with what has been observed in case of carbon nanotubes in water.[26−28] As even the most hydrophobic regions in a protein have significant polarity and dispersion interactions, these studies demonstrate the importance of taking into consideration such interactions in dealing with hydrophobicity induced protein folding and aggregation. Given this level of understanding of the equilibrium situation the dynamical time scales on which the molecular exchanges occur become important to our mechanistic understanding.

Recent advancement in experimental techniques such as nuclear magnetic relaxation dispersion (NMRD),[29,30] inelastic neutron scattering (INS),[31] infrared (IR) spectroscopy,[32] etc. has made it possible to study structure and dynamics of hydration water in the vicinity of large solutes. In particular, the rotational and translation diffusions and the residence time of water confined to the solvation shell of a large biomolecule have been the subject of many recent investigations involving experiments[29,31,32] as well as simulations.[33,34−36] Although the results from different INS studies[31] are not completely consistent, NMRD techniques have provided a more unified picture of the diffusion of water around a protein.

Molecular dynamics (MD) simulation on the other hand can provide a detailed picture of model molecular motions leading to the macroscopic variables such as NMR relaxation times and molecular diffusion rates. The dynamical insight from simulation helps in characterizing the perturbation of the solvent rotational and translation diffusion caused by the presence of the solutes. The early study[35] of solvent molecular dynamics in regions of hydrophobic hydration of two small solutes has shown how water translational and orientational motion can be affected by the close proximity of the nonpolar solutes. Of late, there are a number of simulation studies[33,34,36] and combined INS and MD studies[37,38] concerning the dynamics of the hydration water of a protein molecule. It has been shown that dynamical properties of hydration waters close to the protein surface are markedly different from those of the bulk water. These studies have shown that relaxation behavior of many dynamical quantities deviates significantly from the bulk exponential decay. These MD studies reveal two types of time constants with anomalous relaxation behavior, as observed in highly heterogeneous disordered systems such as supercooled liquids.

In our previous study[24] on the hydration behavior of two large hydrophobic model solutes, we have calculated the equilibrium free energy profile or the potential of mean force (PMF) between two nanoscopic hydrophobic plates. In the free energy profile we found three local minima in addition to the contact pair state. Examination of the solute−solvent structure corresponding to these three minima apart from the contact minimum reveal that these three minima correspond to three different solute−solvent state corresponding to one, two and three intervening water layers between the two solutes.

In the present study we investigate the dynamical properties of the water confined between these two solutes at these three intersolute distances. It is interesting to consider not only how different the dynamical behavior of these water molecules in various size traps is from that of the bulk but also how similar their behavior is with the water near a protein surface or other model surfaces.

II. Method

In the present work, we shall first briefly recall the procedure used previously.[24] The interested reader can find more details in that work.[24] Here we consider the dynamical properties of water between two large, flat hydrophobic solutes by MD simulation in a constant pressure ensemble. Each of the hydrophobic solutes considered here was modeled as a graphite-like sheet or plate made up of 60 carbon atoms placed in hexagonal lattice with carbon−carbon bond lengths of 1.4 Å, with the dimension of 11 Å × 12 Å. The water molecule in this study was represented by the standard SPC/E[39] model. The two sheets were placed symmetrically around the center of a cubic box containing 1800 water molecules, with the plates being parallel to each other as well as to the *xy*-plane with three fixed intersolute distances r_0 corresponding to three solvent separated states represented by three local minima in the potential of mean force calculated in our previous study. The carbon atoms of the solutes were modeled as uncharged particles having intermolecular interactions via a Lennard-Jones (LJ) potential with diameter $\sigma_{CC} = 3.4$ Å and a well depth $\epsilon_{CC} = 0.086$ kcal mol $^{-1}$ (or 0.3598 kJ mol^{-1}), corresponding to the sp^2 carbon atoms in the AMBER 96 force field.[25] The usual Lorentz−Berthelot mixing rules [$\sigma_{OC} = (\sigma_{CC} + \sigma_{OO})/2$ and $\epsilon_{OC} = (\epsilon_{CC}\epsilon_{OO})^{1/2}$, with σ_{OO} and ϵ_{OO} being the LJ parameters for oxygen atoms of SPC/E water] were employed to calculate the interaction parameters for solute−water interactions. The solutes were kept fixed at specific intersolute separations corresponding to the three previously found minima in the solute−solute potential of mean force. Simulations in the isothermal isobaric (NPT) ensemble were carried out using the molecular dynamics (MD) extended system approach of Nose' and Anderson.[40−42] Periodic boundary conditions were applied and all electrostatic interactions were calculated using the Ewald method.[43] The bonds and angles between oxygen and hydrogen atoms of the water molecules were constrained by use of the RATTLE algorithm,[43,44] and the solutes were kept rigid. All the systems were simulated at a target pressure of 1 atm and a target temperature of 298 K. The equations of motion were integrated using velocity Verlet algorithm[43,45] with a 2 fs time step. Each of these reference states was equilibrated for 100 ps and dynamical properties were calculated from the coordinates and velocities saved at every 0.02 ps (20 fs) for next 400 ps.

The dynamical properties of a fluid are conveniently described through a consideration of a time correlation function $C(t)$,

which can be cast in the form

$$C(t) = \langle \sum_{i=1}^{N} \mathbf{f}_i(t) \cdot \mathbf{f}_i(0) \rangle / \langle \sum_{i=1}^{N} \mathbf{f}_i(0) \cdot \mathbf{f}_i(0) \rangle \quad (1)$$

where $\mathbf{f}_i(t)$ is a vector function of positions or velocities of a molecule i from the set of N molecules at time t. Throughout the present analysis of time correlation functions for water between two solutes, we adopt the convention that a molecule's entire dynamical history is classified according to its positions usually on the basis of spatial proximity at an initial time. Thus in the above equation the sum over N includes only contributions from those molecules that are within the confined space between two solutes at an initial time, irrespective of there actual position at time t later or at any intermediate time between 0 and t. Therefore we rewrite eq 1 for the present case as

$$C(t) = \frac{1}{\Omega} \langle \sum_{i=1}^{N} \mathbf{f}_i(t) \cdot \mathbf{f}_i(0) \rangle = \frac{1}{\Omega} \left[\frac{1}{t_0^{\max}} \sum_{t_0=1}^{t_0^{\max}} \frac{1}{N_{\text{occu}}} \sum_{i=1}^{N} [\mathbf{f}_i(t_0) \cdot \mathbf{f}_i(t_0+t)] \theta_i(t_0) \right] \quad (2)$$

where the function $\theta_i(t_0)$ is 1, if molecule i is within the confined region at an initial time irrespective of its position at any other time, and 0 otherwise. Ω in the above equation is the normalization constant given by

$$\Omega = \frac{1}{t_0^{\max}} \sum_{t_0=1}^{t_0^{\max}} \frac{1}{N_{\text{occu}}} \sum_{i=1}^{N} |\mathbf{f}_i(t_0)|^2 \theta_i(t_0) \quad (3)$$

where $t_0^{\max}$ is the total number of time origins considered for time averaging and N_{occu} is the number of molecules in the confined space averaged over all the time origins. As mentioned by Zichi et al.,[35] this specific classification scheme avoids the introduction of a bias that would necessarily be imposed by a scheme[46] that calculates the dynamical properties in confined space or shell region considering only those molecules that remain in the region of interest at least as long as the greatest correlation time considered. Although short time dynamical behavior will be well characterized by this scheme,[46] as one would not expect most of the molecules to migrate from the confined region at short time, long time dynamical behavior may not reflect correct behavior, because this scheme does not take into consideration the crossing of molecules through the shell boundary that dominates at longer times. The present scheme, however, avoids this difficulty. The power spectrum for the velocity autocorrelation function has been obtained from the Fourier transformation of the velocity autocorrelation function using Filon's method.[43]

III. Results and Discussion

In our previous investigation[24] we have determined the PMF between two large atomistic hydrophobic plates as described above and we have shown that apart from the contact pair state at an intersolute distance (r_0) of around 3.4 Å, there are three local minima corresponding to the three solvent separated states with one, two and three intervening water layer/s at separations r_0 of 6.8 Å (state A), 9.8 Å (state B), and 13.0 Å (state C), respectively. In the present study, we describe the dynamical behavior of the intervening water molecules for these three states. First we shall describe a time correlation function that describes the dynamical behavior of the occupation of the intersolute regions by the solvent water, which is known as occupation time distribution function.[35] Then we will analyze the translational diffusion of these water molecules both from the short time behavior given by the velocity autocorrelation function and also from the longer time mean square displacement. The rotational mobility will be analyzed by calculating both first and second rank rotational correlation functions of the water dipoles.

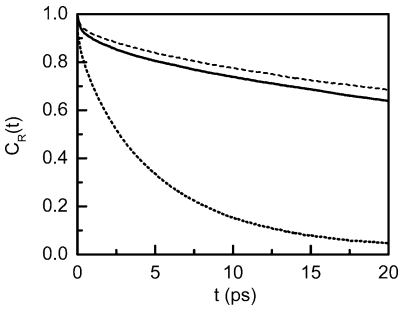

Figure 1. Occupation time distribution functions for the water molecules belonging to three different confined states. The dashed line is for state A with $r_0 = 6.8$ Å, the solid line is for state B with $r_0 = 9.8$ Å, and the dotted line is for state C with $r_0 = 13.0$ Å.

A. Occupation Time Distribution Function. The occupation time distribution function is calculated here from the time correlation function of the form represented by eq 1 with $f_i(t)$ (or $f_i(0)$) equal to 1 if a water molecule i is in the confined region between two solutes at time t (or at time 0), otherwise $f_i(t)$ (or $f_i(0)$) is set equal to zero. Notice that a molecule which leaves the region of interest at any time t, on reentering the region, can continue to contribute to the distribution at any later time. Thus we can write a normalized occupation time distribution function $R(t)$ as

$$R(t) = \frac{1}{\Omega} \left[\frac{1}{t_0^{\max}} \sum_{t_0=1}^{t_0^{\max}} \frac{1}{N_{\text{occu}}} \sum_{i=1}^{N} \theta_i(t_0)\, \theta_i(t_0+t) \right]$$

with

$$\Omega = \frac{1}{t_0^{\max}} \sum_{t_0=1}^{t_0^{\max}} \sum_{i=1}^{N} \theta_i(t_0)\, \theta_i(t_0) \quad (4)$$

where $\theta_i(t) = 1$, if the oxygen atom of a water molecule i is in the region of interest at time t and zero otherwise. In Figure 1 we have shown $R(t)$ of water as a function of time for three intersolute separations $r_0 = 6.8$ Å (state A), 9.8 Å (state B) and 13.0 Å (state C). The function $R(t)$ as defined by eq 4 measures the probability that the confined region is occupied by a water molecule for a time $t + \mathrm{d}t$ on average and its decay with time provides information about the local dynamics of the hydration water molecules. As seen in Figure 1, all the three occupation time distribution functions $R(t)$ decay initially very rapidly followed by a slower decay. The nature of these time profiles indicates that at least two time scales are required to describe the relaxation processes over the entire period of time. Although a biexponential relaxation is often employed to describe such a decay, a single exponential for the fast dynamics and a stretched exponential for the long time (slower) relaxation in the present case fits the calculated data with considerably better precision, e.g.

$$R(t) = A e^{-(t/\tau_l)^{\beta_l}} + B e^{-t/\tau_s} \quad (5)$$

TABLE 1: Fitting Parameters for the Occupation Distribution Time Correlation Function *R*(*t*) As Calculated Using Eq 4 and Fitted to a Curve According to Eq 5

r_0 (Å)	A	τ_l (ps)	β_l	B	τ_s (ps)
6.8 (state A)	0.96 ± 0.0004	102.6 ± 0.278	0.66 ± 0.002	0.04 ± 0.0004	0.15 ± 0.004
9.8 (state B)	0.95 ± 0.0005	86.5 ± 0.245	0.65 ± 0.002	0.05 ± 0.0005	0.19 ± 0.004
13.0 (state C)	0.92 ± 0.0007	4.9 ± 0.006	0.81 ± 0.0009	0.08 ± 0.0007	0.015 ± 0.001

where τ_s and τ_l are the two time constants associated with short and long time decay, respectively, β_l being the stretch-exponent for the long time decay. This behavior is not uncommon in systems that are characterized by complicated length and time scales.[47] The two preexponents A and B in the above equation are the measure of the relative proportions of the long and short time processes, respectively. The stretched exponential behavior, referred to as the Kohlrausch−Williams−Watts (KWW) law, is often employed in the characterization of the non exponential nature of relaxations in several phenomena in condensed matter systems such as supercooled liquids and protein folding. The KWW time constant provides the time scale over which the process evolves. In the present case it gives us average time over which the confined region is occupied by an average water. The exponents β_l in the above equation is the signature of the deviation of the dynamics in disordered media from a simple exponential law. The deviation of β_l from unity signifies the deviation of the relaxation from the usual exponential behavior. A fast initial relaxation due to the presence of a transient librational phenomenon follows a simple single-exponential decay, whereas the slower long time relaxation is well fit with a stretched exponential decay. This type of behavior with two time constants has also been observed in many recent studies[33,34,36] involving residence time of hydration water near a protein surface and in many other different relaxation processes.[47,48]

The values of all the parameters related to this decay for the three occupation distribution functions considered here are given in Table 1. The examination of these values shows that at $r_0 =$ 6.8 Å (state A), where two solute plates are separated by a single layer of water molecules, the long nonexponential relaxation process is very slow with a large time constant of around 100 ps. In the case of $r_0 = 9.8$ Å (state B) also, where the intersolute region is occupied by two layers of water, we find the relaxation time for the slow (long time) process to be fairly large, but smaller than the first case, which signifies that water in state A is less mobile than that in state B. For $r_0 = 13$ Å (state C); however, we find the long time decay constant to be much smaller than that in the previous two cases, indicating that water in this state is much more free as compared to other two cases.

The β_l parameters indicate the degree of stretched exponential behavior. We note that the for states A and B β_l is significantly smaller than for state C. This indicates that though states A and B have a significant KWW process in the relaxation, state C demonstrates less complicated dynamics in the long time process.

The fast dynamics show a small overall contribution to the curve as noted by the coefficients, which are less than 10% of the total in all cases. The fast decay processes, which last only fractions of a picosecond, are very similar for states A and B, but for state C this process decays much faster as compared to A and B state. The fast transient in $R(t)$ is due to very local librational motions of a water molecule in a cage formed by its surrounding neighbors. The comparatively slower decay of this fast process for states A and B as compared to states C signifies that local environment of a water in states A and B are much more rigid due to the close proximity of the two large solute surfaces and pronounced structure formation in this region. The relative proportions of the short and long time processes as indicated by the values of the coefficients reveal that the overall decay process is dominated by the long time process for all the three states.

B. Translational Motion and Diffusion of Water Molecules. *1. Velocity Autocorrelation Function of Water Molecules.* The velocity autocorrelation function (VCF) has long been used to reveal dynamics in the liquid state.[49] Here, we use it as a sensitive measure of the effects of confinement on the trapped water molecules between the plates. It is calculated for the three states A, B and C considered here by extending the definition of time correlation function given by eqs 1−3, viz.,

$$C_v(t) = \frac{\langle \mathbf{v}(t)\cdot\mathbf{v}(0)\rangle}{\Omega} = \frac{1}{\Omega}\left[\frac{1}{t_0^{\max}}\sum_{t_0=1}^{t_0^{\max}}\frac{1}{N_{occu}}\sum_{i=1}^{N}\{\mathbf{v}_i(t_0)\cdot\mathbf{v}_i(t_0+t)\}\theta_i(t_0)\right]$$

with

$$\Omega = \frac{1}{t_0^{\max}}\sum_{t_0=1}^{t_0^{\max}}\frac{1}{N_{\mathrm{occu}}}\sum_{i=1}^{N} v_i(t_0)^2\,\theta_i(t_0) \qquad (6)$$

where $\mathbf{v}_i(t)$ is the velocity vector for the oxygen atom of the i th water molecule at time t and $\theta_i(t_0)$ is 1, if the ith water molecule is in the confined region at time origin t_0 irrespective of its position at time t later. Thus in the sum over N in the above equations we only include the velocities of those molecules that are present in the confined region at the initial time t_0, a time origin. The velocity correlation functions for states A, B, and C are presented in Figure 2a. The velocity correlation function for states B and C are quite similar to each other and are close to bulk water, whereas that for state A is strikingly different from the same for other two states. For states B and C, after a quick initial decay, a small minimum and shoulder are observed due to rebound of the molecules from the shell of their neighbor. This type of behavior is also observed in the water near protein surfaces[33,34,36] and for two hydrophobic solutes[35] in water. Notice that this feature is suppressed for state A, in which water molecules are correlated with the solutes. The oscillations in the VCF are generally due to the manifestation of the many body correlations and the differences in the oscillations observed in these three cases indicate that waters are in spatially different environments. The negative dip and subsequent strong oscillations for $r_0 = 6.8$ Å case (state A) are indicative of larger confinement effect in this case.

We compare the VCF of the multilayered state C with that of bulk water, in the inset of Figure 2a. They are obviously similar. The decay of the VCF has been achieved within roughly 1 ps for states B and C, whereas the oscillation persisted for almost 1.5 ps for state A. Thus the diffusive regime by this measure starts from 1 ps onward for states B and C and beyond 1.5 ps for state A. This general time scale was seen in earlier analyses of water dynamics near protein surfaces.[50]

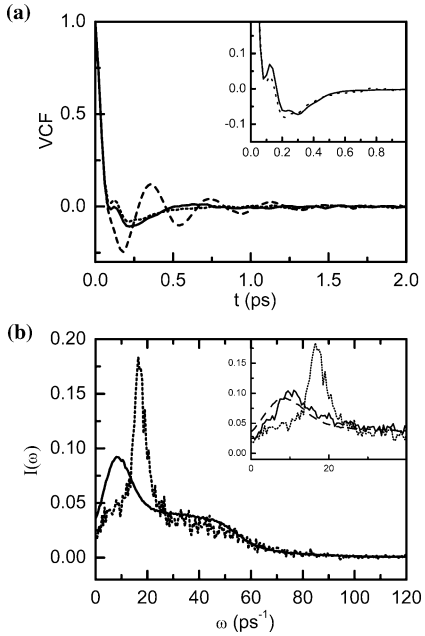

Figure 2. (a) Velocity−velocity autocorrelation functions for the water oxygens belonging to the three confined regions. Legends are the same as in Figure 1. Inset: VCF for bulk water is shown by solid line along with the same for state C shown by dotted lines. (b) Power spectra obtained from the Fourier transform of the velocity−velocity autocorrelation functions for the water oxygens belonging to the bulk water (solid line) and state A with $r_0 = 6.8$ Å (dotted line). Inset: power spectra for states A (dotted line), B (solid line), and bulk (dashed line).

TABLE 2: Diffusion Coefficients of Water in States A, B, C and bulk from the Velocity Autocorrelation Integral (Eq 7) as Well as from the Slope of Mean Square Displacement (Eq 8) and α Values from the Fitting of the MSD Plot to Eq 9

	$D/10^{-5}$ (cm^2/s)		
r_0 (Å)	from VCF	from MSD	α
6.8 (state A)	1.22	1.17	0.89 ± 0.001
9.8 (state B)	1.83	1.83	0.96 ± 0.002
13.0 (state C)	2.57	2.54	0.96 ± 0.001
∞ (bulk)	3.05	2.86	0.96 ± 0.0005

The calculation of the diffusion constant (D) from the integration of the VCF using relation

$$D = \frac{1}{3}\int_0^\infty \langle \mathbf{v}(t)\cdot\mathbf{v}(0)\rangle \, \mathrm{d}t \tag{7}$$

for three states are performed by numerically integrating the corresponding VCF; the values are tabulated in Table 2 along with that calculated from mean square displacement (discussed below). The upper limit of the integration for state A has been set to 2 ps, where as those for states B and C have been set to 1.5 ps.

The power spectrum obtained by Fourier transformation of the velocity autocorrelation function is presented in Figure 2b. The frequency spectrum for the bulk water shown by solid line has a major peak around 9−10 ps^{-1}, attributed to manybody motions[35] and a broad shoulder-like peak at around 40−45 ps^{-1}, attributed to pairwise intermolecular oxygen−oxygen vibrations[51,52] and is in good agreement with a recent study[53] on bulk water as well as that from early computer simulations of water.[51] The frequency spectrum for state A shown by the dotted line reveals a large shift of the 9−10 ps^{-1} bulk water peak to a much higher frequency of around 16−17 ps^{-1} for our confined system. The frequency distributions in the power spectrum are indicative of the relative population of the density of states of independent

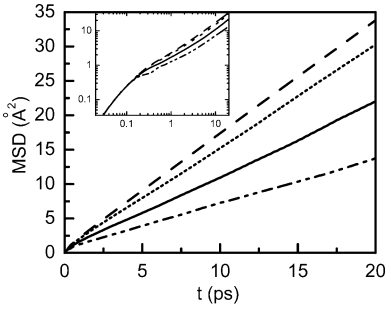

Figure 3. Mean square displacements of water oxygens from the three confined regions and the same for bulk. The dashed line is for bulk water, the dotted line is for state C with $r_0 = 13.0$ Å, the solid line is for state B with $r_0 = 9.8$ Å, and the dash-double dotted line is for state A with $r_0 = 6.8$ Å. Inset: plots of the same MSDs in the log−log scale.

oscillators corresponding to a particular frequency, related here to the local motions of water molecules. The shift in the main peak for state A toward higher frequency can be attributed to a larger forces acting on the molecules imparted by the restrictive environment in this state. For comparison in the inset of the same figure we have shown the power spectra for state B denoted by solid line, state A denoted by dotted line and bulk water shown by dashed line. A very small shift of 1−2 ps^{-1} in the first peak for state B from the same for bulk water is observed, whereas the same for state C although not shown here for clarity are almost identical as that for state B. Spectra for all the confined states are noisy due to poor statistics caused by the small number of water molecules between the two solutes.

2. Mean Square Displacement of Water Molecules. The mean square displacement (MSD) ($\langle \Delta r^2 \rangle$ of the water oxygen for the three states A, B, and C as well as for bulk water are shown in Figure 3. As all other time correlation functions, MSD also has been calculated by averaging over only those water molecules that are in the confined region at the initial time (i.e., time origin t_0). The mean square displacement is a good measure of the water translational mobility in a given environment and therefore gives us information about the diffusion processes in the medium. The MSD at long times is related to the self-diffusion coefficient (D) of water by the well-known Einstein relation

$$D = \frac{1}{6}\lim_{t\to\infty}\frac{\langle \Delta r^2 \rangle}{\Delta t} = \frac{1}{6}\lim_{t\to\infty}\frac{\langle |\mathbf{r}(t) - \mathbf{r}(0)|^2 \rangle}{\Delta t} \tag{8}$$

where $\mathbf{r}(t)$ is the position vector at time t. The diffusion constants are obtained for each of the three states considered here and bulk water from the slope of a linear fit of the respective MSD data calculated from simulation trajectory. Comparing all the MSDs presented in Figure 3, we see that slope of MSD for state A is the smallest one and it increases as we go to larger intersolute distances of 9.8 and 13 Å in states B and C, respectively. The slope of the MSD for state C is very close to that for bulk water indicating that the water in state C is not so perturbed by the confinement due to solutes. This might be unexpected given the strong density waves that exist for this state.[24] Thus the diffusion constant is the lowest for the confined water molecules in state A and it increases with an increase in the volume of the confined space. The diffusion constants as obtained from integration of the VCF also show same trend. The diffusion constants as obtained from MSDs are displayed in Table 2.

The smaller diffusion constant for state A as compared to bulk water is due to the lower mobility of water in the confined region. The temperature of the confined water in state A as

calculated from the average kinetic energy of these confined water molecules from our simulation trajectory is around 10 K less than the average temperature lagging the entire system. Though the trend indicates an energy loss mechanism, the details are an artifact related to the particular implementation of the Nose′ style temperature bath. A similar temperature decrease for the intersolute water has also been observed by Zichi et al. in the NVE ensemble.[35] This finding may have implication in the role of solvent mobility on the protein glass transition.[54]

To examine whether any anomalous diffusion phenomenon, as observed in many studies[33,34,36,48] on hydration water of proteins, exists in any of the present cases, we present the same MSD plot in log−log scale in the inset of Figure 3. Initially, up to around 0.2 ps, the behavior of the MSD for all three states is almost indistinguishable. In this time zone the diffusive regime has not been reached. Beyond this point, however, all the three MSDs are different from each other, indicating a different diffusive environment in each of the three states. As seen in the VCF plot, the diffusive regime is established for states B and C within around 1 ps, and for state A around 1.5 ps. Beyond these times where diffusive regimes have fully been established, the MSDs in the log−log plot (inset) appear to be linear with time. The slope for state A is smaller than that corresponding to normal diffusion, which obeys linear relation $\langle \Delta r^2 \rangle \sim t^1$. The deviation from linearity of the solvent MSD has also been observed in hydration water of protein molecules. To measure the deviation from normal linear behavior of MSD, it is generally fitted with the equation

$$\langle \Delta r^2 \rangle \propto t^{\alpha} \tag{9}$$

The exponent α is a measure of the deviation from the linear behavior. The value of α is 1 in the ideal case of 3-D Brownian diffusion, and any deviation from unity indicates the presence of anomalous diffusion sometimes related to a change in effective dimensionality. In the case of the hydration water of a protein molecule the value of α is usually less than 1 and this sublinear behavior is attributed to the highly hindered motion of the solvent molecules due to the presence of large solute around them and also due to the enhanced solvent structure formed around solute molecule to gain stability.

For our idealized system of confined water between plates, the values of α have been extracted from the simple fit of the MSD in the log−log plot by eq 9 and are tabulated in Table 2. For state A, where only a single layer of water is trapped between two large solutes, the model water molecules are highly structured and thus the smaller value of $\alpha = 0.89$ indicates that diffusion behavior in this region deviates significantly from the normal behavior. For the other two states α values are close to 1, indicating almost normal diffusion.

C. Rotational Diffusion of Water Molecules. The rotational diffusion of the water molecules in the region between two solutes with three intersolute separations corresponding to our defined states A, B, and C has been analyzed through the reorientational dynamics of dipole moment vectors μ. The time evolution of μ can easily be determined by calculating the autocorrelation functions Γ_1 defined as the autocorrelation of the Legendre polynomials $P_l(\cos\theta(t))$. Thus, we have

$$\Gamma_l(t) = \langle P_l(\hat{\mu}(0)\cdot\hat{\mu}(t)) \rangle \tag{10}$$

where $\hat{\mu}(t)$ is the unit vector along the dipole moment vector at time t. The first ($l = 1$) and second ($l = 2$) order Legendre polynomial are calculated from our MD simulation and can also be obtained from experiments. First-order properties can be

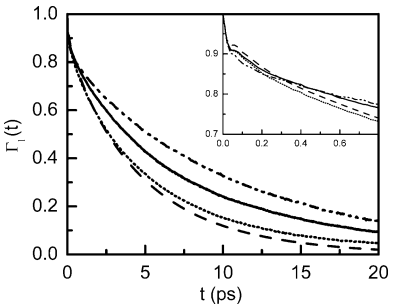

Figure 4. First-order reorientational correlation functions $\Gamma_1(t)$ (see eq 10 with $l = 1$) of the dipoles of water molecules in three different confined environments corresponding to states A, B, and C and in bulk. Inset: same plot with magnification of initial times. Legends are the same as in Figure 3.

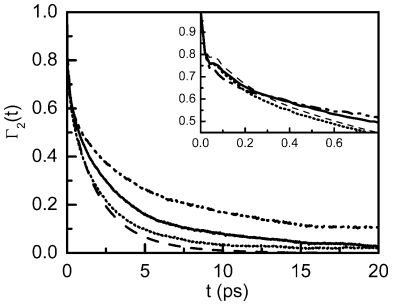

Figure 5. Second-order reorientational correlation functions $\Gamma_2(t)$ (see eq 14 with $l = 2$) of the dipoles of water molecules in three different confined environments corresponding to states A, B, and C and in bulk. Inset: same plot with magnification of initial times. Legends are the same as in Figure 3.

derived from the infrared spectroscopy, whereas the second-order function is obtained from NMR experiments. We present $\Gamma_1(t)$ in Figure 4 and $\Gamma_2(t)$ in Figure 5 for the present case of confined water in three states A, B, and C along with the same for bulk water. In general Γ_2 decays much faster than Γ_1 for all the four cases studied here. The long time decay of both Γ_1 and Γ_2 also follow the same general trend that a longer time is required for relaxation in the case of stronger confinements as in state A with $r_0 = 6.8$ Å and relaxation becomes faster in going to larger r_0 values. Thus both these functions indicate that confinement makes the rotational rearrangement hindered in confined spaces. Similar behavior has also been observed in case of hydration water of some globular proteins,[33,34,36] where the close proximity of water to the protein surface has made the reorientation slower. At very short time a quick initial decay followed by a bump as seen in the inset of Figure 4 corresponding to the librational oscillations is finally superimposed upon a long time decay. This behavior was also observed earlier[35] for water between two small hydrophobic solutes. Due to the existence of two time scales a single exponential or single stretched exponential decay cannot describe well the calculated data over the entire time range. In the present case, we find that a stretched exponential for short time decay and a simple single exponential for long time process for both the Γ_1 and Γ_2 in all the four cases can describe the calculated result over the entire time scale of 0 to 20 ps considered here. The form of the equation with which both Γ_1 and Γ_2 have been fitted is as follows:

$$\Gamma_l(t) = A e^{-(t/\tau_s)\beta_s} + B e^{-(t/\tau_l)} \tag{11}$$

where τ_s and τ_l are the relaxation times corresponding to short and long time processes, β_s corresponds to the stretching exponents for short time process and A and B are the relative

TABLE 3: Fitting Parameters Obtained from the Fitting of the Rotational Correlation Function $\Gamma_1(t)$ to a Curve According to Eq 11

r_0 (Å)	A	τ_s (ps)	β_s	B	τ_l (ps)
6.8 (state A)	0.25 ± 0.001	0.53 ± 0.018	0.30 ± 0.003	0.75 ± 0.001	11.19 ± 0.023
9.8 (state B)	0.34 ± 0.002	3.16 ± 0.033	0.31 ± 0.003	0.66 ± 0.002	7.05 ± 0.015
13.0 (state C)	0.36 ± 0.002	2.05 ± 0.014	0.38 ± 0.002	0.64 ± 0.002	5.27 ± 0.007
∞ (bulk)	0.24 ± 0.0008	0.89 ± 0.008	0.39 ± 0.002	0.64 ± 0.0008	4.93 ± 0.004

TABLE 4: Fitting Parameters Obtained from the Fitting of the Rotational Correlation Function $\Gamma_2(t)$ to a Curve According to Eq 11

r_0 (Å)	A	τ_s (ps)	β_s	B	τ_l (ps)
6.8 (state A)	0.76 ± 0.0030	1.31 ± 0.017	0.27 ± 0.0020	0.24 ± 0.0030	4.71 ± 0.033
9.8 (state B)	0.67 ± 0.0034	0.73 ± 0.012	0.33 ± 0.0023	0.33 ± 0.0034	3.07 ± 0.013
13.0 (state C)	0.62 ± 0.0029	0.44 ± 0.007	0.34 ± 0.0021	0.38 ± 0.0029	1.90 ± 0.007
∞ (bulk)	0.51 ± 0.0019	0.28 ± 0.004	0.43 ± 0.0021	0.49 ± 0.0019	2.17 ± 0.006

proportions of the two processes, respectively. The values of the time constants (τ) and stretched exponents for both Γ_1 and Γ_2 are displayed in Table 3 and 4, respectively. As expected the decay for the slower process in both Γ_1 and Γ_2 becomes slower with decreasing values of r_0 corresponding to greater confinement. However, the fast process for $r_0 = 6.8$ Å (state A) in Γ_1 shows a rapid decay compared to other two states. This is also evident from the plot in the inset of Figure 4, which shows that in this time scale (0−0.3 ps), state A decays faster compared to other states.

In general we find the more confinement, the more the restrictions in motion, both rotational and translational. This result is in contrast to the notion that water might not only attempt to dewet but also be more mobile in proximity to surfaces.

IV. Conclusions

In the present work we have investigated the effect of two large hydrophobic solutes on the dynamical behavior of water between two solutes. The water between the two solutes are in close proximity to both the solutes and are thus likely the most perturbed water in the whole system. The longer occupation time of water in the smallest confined region studied here (state A) indicates that water in this region is highly structured. A similar inference can be drawn from the VCF and RMSD calculations. With the increase in volume of the confined region dynamics of water becomes faster in general. Analysis of occupation time distribution function and rotational correlation functions indicate two time scales with two distinct relaxation times. The sublinear trend in the MSD and stretched relaxation in many of the dynamical processes indicate anomalous dynamical relaxation reminiscent of hydration water near the protein surfaces[33] and supercooled liquids.[48] Thus the present study shows that the behavior of water near the large hydrophobic model plates considered here has been significantly perturbed by the presence of the big solutes, in the same way as that expected for the hydration water of proteins.

Acknowledgment. We thank L. R. Pratt, A. D. J. Haymet, G. C. Lynch and K.-Y. Wong for many valuable technical discussions. We gratefully acknowledge the NIH, the R. A. Welch foundation, and TiiMES, funded by NASA Cooperative Agreement No. NCC-1-02038 for partial financial support of this work. The computations were performed in part using the NSF meta center facilities and the Molecular Science Computing Facility in the W. R. Wiley Environmental Molecular Sciences Laboratory, a national scientific user facility sponsored by DOE's Office of Biological and Environmental Research and located at Pacific Northwest National Laboratory, operated for DOE by Battelle.

References and Notes

(1) Kauzmann, W. *Adv. Protein Chem.* **1959**, *14*, 1.
(2) Lounnas, V.; Pettitt, B. M.; Philips, G. N., Jr. *Biophys. J.* **1994**, *66*, 601.
(3) Makarov, V. A.; Andrews, B. A.; Pettitt, B. M. *Biophys. J.* **1998**,*74*, 413.
(4) *Protein−Solvent Interactions*; Gregory, R. B., Ed.; Dekker: New York, 1995.
(5) Pal, S. K.; Peon J.; Zewail, A. H. *Proc. Natl. Acad. Sci U.S.A.* **2002**, *99*, 1763.
(6) Kauntz, I. D.; Kauzmann, W. *Adv. Protein Chem.* **1974**, *28*, 239.
(7) Poole P. L.; Finney, J. L. *Biopolymers* **1983**, *22*, 255.
(8) Rupley J. L.; Careri, G. *Adv. Protein Chem.* **1991**, *41*, 37.
(9) Makarov, V. A.; Pettitt, B. M.; Feig, M. *Acc. Chem. Res.* **2002**, *35*, 376−384.
(10) Makarov, V.; Andrews, K.; Smith, P.; Pettitt, B. M. *Biophys. J.* **2000**, *79* 2966−2974.
(11) Lum, K.; Chandler D.; Weeks, J. D. *J. Phys. Chem. B* **1999**, *103*, 4570.
(12) Pratt, L. R.; Pohorille, A. *Chem. Rev.* **2002**, *102*, 2671.
(13) Tanford, C. *The Hydrophobic Effect: Formation of Micelles and Biological Membranes*; John Weiley: New York, 1973.
(14) Tanford, C. *Protein Sci.* **1997**, *6*, 1358.
(15) Tanford, C. *Science* **1978**, *200*, 1012.
(16) Dill, K. A. *Biochemistry* **1990**, *29*, 7133.
(17) Huang, D. M.; Chandler, D. *Proc. Natl. Acad. Sci. U.S.A.* **2000**, *97*, 8324.
(18) Huang, D. M.; Geissler, P. L.; Chandler, D. *J. Phys. Chem. B* **2001**, *105*, 6704.
(19) Huang, D. M.; Chandler, D. *J. Phys. Chem. B* **2002**, *106*, 2047.
(20) Wallqvist, A.; Berne, B. J. *J. Phys. Chem.* **1995**, *99*, 2885.
(21) Wallqvist A.; Berne, B. J. *J. Phys. Chem.* **1995**, *99*, 2893.
(22) Huang, X.; Margulis C. J.; Berne, B. J. *Proc. Natl. Acad. Sci. U.S.A.* **2003**, *100*, 11953.
(23) ten Wolde, P. R.; Chandler, D. *Proc. Natl. Acad. Sci. U.S.A.* **2002**, *99*, 6539.
(24) Choudhury, N.; Pettitt, B. M. *J. Am. Chem. Soc.*, in press.
(25) Cornell, D. W.; Cornell, W. D.; Cieplak, P.; Bayly, C. I.; Gould, I. R.; Merz, K. M.; Ferguson, D. M.; Spellmeyer, D. C.; Fox, T.; Caldwell J. W.; Kollman, P. A. *J. Am. Chem. Soc.* **1995**, *117*, 5179.
(26) Hummer, G.; Rasaiah, J. C.; Noworyta, J. P. *Nature* **2001**, *414*, 188.
(27) Sansom M. S. P.; Biggin, P. C. *Nature* **2001**, *414*, 156.
(28) Kalra, A.; Garde, S.; Hummer, G. *Proc. Natl. Acad. Sci. U.S.A.* **2003**, *100*, 10175.
(29) Polnaszek, C. F.; Bryant, R. G. *J. Am. Chem. Soc.* **1984**, *106*, 428. Danisov V. P.; Halle, B. *Faraday. Discuss.* **1996**, *103*, 227. Halle, B. In *Hydration Processes in Biology*; Bellissent-Funel, M.-C., Ed; IOS Press: Ohmsha, 1999.
(30) Danisov, V. P.; Jomsson B. H.; Halle, B. *Nat. Struct. Biol.* **1999**, *6*, 253.
(31) Bellissent-Funel, M. C.; Teixeria, J.; Brandley, K. F.; Chen S. H.; Crespi, H. L. *Physica B* **1992**, *180−181*, 740. Settles M.; Doster, W. *Faraday. Discuss.* **1996**, *103*, 269. Zanotti J.-M.; Chen, S. H. *Faraday. Discuss.* **1996**, *103*, 281. Dellerue, S.; Bellissent-Funel, M. C. *Chem. Phys.* **2000**, *258*, 315.
(32) Zubavicus, Y.; Grunze, M. *Science* **2004**, *304*, 974. Wernet, P.; Nordlund, D.; Bergmann, U.; Cavalleri, M.; Odelius, M.; Ogasawara, H.; Naslund, L. A.; Hirsch, T. K.; Ojamae, L.; Glatzel, P.; Pettersson L. G. M.; Nilsson, A. *Science* **2004**, *304*, 795. Schultz, C. P. *Nat. Struct. Biol.*

2000, *7*, 7. Troullier, A.; Reinstadle, D.; Dupont, Y.; Naumann D.; Forge, V. *Nat. Struct. Biol.* **2000**, *7*, 78.
(33) Bizzarri A. R.; Connistraro, S. *J. Phys. Chem. B* **2002**, *106*, 6617. Rocchi, C.; Bizzarri A. R.; Connistraro, S. *Phys. Rev. E* **1998**, *57*, 3315.
(34) Ghosh Dastidar, S.; Mukhopadhyay, C. *Phys. Rev. E* **2003**, *68*, 021921.
(35) Zichi, D. A.; Rossky, P. J. *J. Chem. Phys.* **1986**, *84*, 2814.
(36) Marchi, M.; Sterpone F.; Ceccarlli, M. *J. Am. Chem. Soc.* **2002**, *124*, 6787.
(37) Sorenson, J. M.; Hura, G.; Soper, A. K.; Pertsemlidis, A.; Head-Gordon, T. *J. Phys. Chem. B* **2004**, *86*, 1852.
(38) Russo, D.; Hura G.; Head-Gordon, T. *Biophys. J.* **2004**, *86*, 1852.
(39) Berendsen, H. J. C.; Grigera, J. R.; Straatsma, T. P. *J. Phys. Chem.* **1987**, *91*, 6269.
(40) Nose, S. *Mol. Phys.* **2002**, *100*, 191.
(41) Andersen, H. C.; *J. Chem. Phys.* **1980**, *72*, 2384.
(42) Nose, S.; Klein, M. L. *Mol. Phys.* **1983**, *50*, 1055.
(43) Allen, M. P.; Tildesley, D. J. *Computer Simulation of Liquids*; Oxford University, New York, 1987.
(44) Andersen, H. C. *J. Comput. Phys.* **1983**, *52*, 24.
(45) Swope, W. C.; Andersen, H. C.; Berens P. H.; Wilson, K. R. *J. Chem. Phys.* **1982**, *76*, 637.
(46) Impey, R. W.; Madden P. A.; McDonald, I. R. *J. Phys. Chem.* **1983**, *87*, 5071.
(47) Yang, W. Y.; Gruebele, M. *Nature*, **2004**, *423*, 193. Snow, C. D.; Nguyen, N.; Pande, V. S.; Gruebele, M. *Nature* **2002**, *420*, 102. Gruebele, M. *Annu. Rev. Phys. Chem.* **1999**, *50*, 485.
(48) Phillips, J. C. *Rep. Prog. Phys.* **1996**, *59*, 1133.
(49) Rahman, A. *Phys. Rev.* **1964**, *136*, A 405.
(50) Lounnas, V.; Pettitt, B. M. *Proteins: Struct., Funct. Genet.* **1994**, *18*, 148−160.
(51) Stillinger, F. H.; Rahman, A. *J. Chem. Phys.* **1971**, *55*, 3336.
(52) Eisenberg, D.; Kauzmann, W. *The Structure and Properties of Water*; Oxford University: Oxford, NY, 1969.
(53) Balucani, U.; Brodholt, J. P.; Vallauri, R. *J. Phys. Condens. Matter* **1996**,*8*, 6139.
(54) Vitkup, D.; Ringe, D.; Petsko, G. A.; Karplus, M. *Nat. Struct. Biol.* **2000**, *7*, 34.